Letter

Multitimescale diffusion in ridepooling dynamics

Philip Marszal [1,*] Nora Molkenthin [2] Marc Timme [1,3,4] and Malte Schröder [1]

[1] Chair of Network Dynamics, Institute of Theoretical Physics and Center for Advancing Electronics Dresden (cfaed), TUD Dresden University of Technology, 01062 Dresden, Germany

[2] Potsdam Institute for Climate Impact Research, Member of the Leibniz Association, 14473 Potsdam, Germany

[3] Center for Synergy of Systems (SynoSys), TUD Dresden University of Technology, 01062 Dresden, Germany

[4] Lakeside Labs, 9020 Klagenfurt, Austria

(Received 8 July 2024; revised 5 May 2025; accepted 16 August 2025; published 29 September 2025)

Diffusion processes and random walks describe the dynamics of systems subject to many unpredictable external influences. Here, we show how trajectories of individual ridepooling vehicles are characterized by a novel type of persistent random walk with a preplanned future route. We find three distinct timescales that reflect short- and long-term alignment and medium-term detours emerging in the routing dynamics, together inducing ballistic, subdiffusive, and diffusive motions of the vehicles. The diffusion constant links the timescales underlying the microscopic dynamics of the routes to macroscopic system parameters such as fleet size and effective demand. Observables quantifying the service quality of ridepooling collapse to a single scaling function of the diffusion constant, directly connecting microscopic timescales to macroscopic properties of system operations.

DOI: 10.1103/bjqt-5vkq

On-demand ridepooling has recently gathered increasing attention from physics and complex systems' sciences, first, because it may offer an efficient transportation mode, and second, because of its intricate dynamics emerging from the interactions between requests and vehicle routes [1–7]. In ridepooling services, customers request door-to-door transport. In response, the system modifies or extends the planned vehicle routes to serve all requests [Fig. 1(a)], similar to conventional taxi services. Unlike in taxi services, however, vehicles may serve several customers at the same time, resulting in a higher vehicle occupancy and ideally facilitating more efficient transportation compared to individual mobility [8–10].

In contrast to public transport line services, the routes of ridepooling vehicles change dynamically [11–14]. Each request adds two new stop locations to the route of one vehicle, one for pickup and one for dropoff. The resulting dynamics of ridepooling systems have so far been computationally evaluated by microscopic agent-based simulations [9,15], empirically analyzed in case studies based on historical data [1,3,16], or theoretically described with the help of macroscopic mean-field models [2,4,17,18]. However, none of these approaches mechanistically links the microscopic dynamics to macroscopically relevant observables.

In this Letter, we change the perspective and show how the microscopic routing dynamics connects to the macroscopic service quality of ridepooling fleets by identifying vehicle trajectories [Fig. 1(b)] as realizations of multitimescale persistent random walks with preplanned future routes.

Consider a fleet of B ridepooling vehicles $j \in \{1, \ldots, B\}$. At any given time t, the state of the ridepooling system is given by the current positions $x_j(t)$ of all vehicles j and their planned future routes $R_j(t)$.

These preplanned routes represent an essential difference between ridepooling vehicle trajectories and common, memoryless random walks [19,20]. The routes consist of future stops $x_{\mathrm{p}}^{(j_k)}$ and $x_{\mathrm{d}}^{(j_k)}$ to pick up (p) and drop off (d) assigned customers j_k. For example, the planned route

$$R_j(t) = \left(x_{\mathrm{p}}^{(j_1)}, x_{\mathrm{p}}^{(j_2)}, x_{\mathrm{d}}^{(j_1)}, x_{\mathrm{d}}^{(j_2)}\right) \tag{1}$$

indicates that customer j_1 is to be picked up first at location $x_{\mathrm{p}}^{(j_1)}$, followed by the pickup of customer j_2. Subsequently, the two customers will be dropped off in the same order at their respective dropoff locations $x_{\mathrm{d}}^{(j_1)}$ and $x_{\mathrm{d}}^{(j_2)}$. These planned routes evolve in two ways [compare Fig. 1(a)]. First, vehicle j may pass its next scheduled stop, shortening its planned route. For instance, the state change (underlined to highlight differences)

$$\left(\underline{x_{\mathrm{p}}^{(j_1)}}, x_{\mathrm{p}}^{(j_2)}, x_{\mathrm{d}}^{(j_1)}, x_{\mathrm{d}}^{(j_2)}\right) \mapsto \left(x_{\mathrm{p}}^{(j_2)}, x_{\mathrm{d}}^{(j_1)}, x_{\mathrm{d}}^{(j_2)}\right) \tag{2}$$

represents the vehicle reaching its next planned stop $x_{\mathrm{p}}^{(j_1)}$ and picking up customer j_1. Second, a new request by a customer r may be assigned to vehicle j, adding both pickup and dropoff locations to its planned route,

$$\left(x_{\mathrm{p}}^{(j_2)}, x_{\mathrm{d}}^{(j_1)}, x_{\mathrm{d}}^{(j_2)}\right) \mapsto \left(x_{\mathrm{p}}^{(j_2)}, x_{\mathrm{d}}^{(j_1)}, \underline{x_{\mathrm{p}}^{(r)}}, x_{\mathrm{d}}^{(j_2)}, \underline{x_{\mathrm{d}}^{(r)}}\right). \tag{3}$$

To understand the fundamental properties of the routing dynamics and to be able to compare them to standard diffusion

*Contact author: philip.marszal@tu-dresden.de

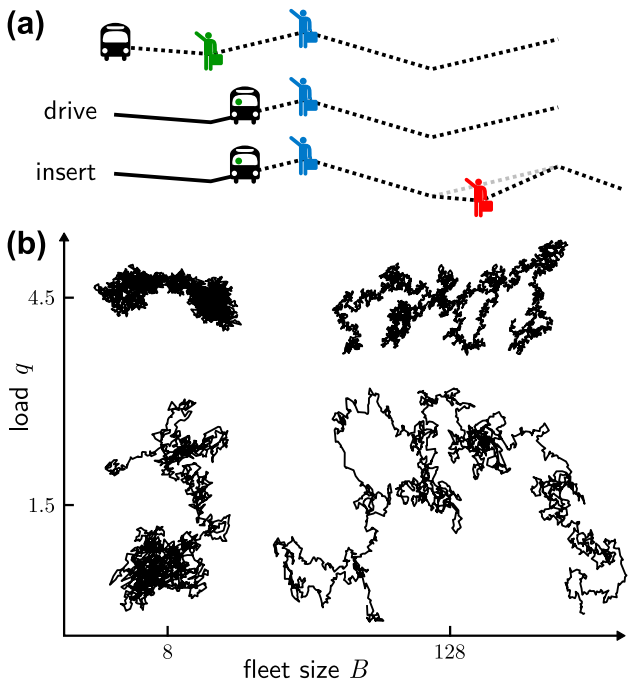

FIG. 1. Ridepooling vehicle trajectories evolve as persistent random walks. (a) Two basic mechanisms change the driven trajectories (solid) and preplanned routes (dotted) of a ridepooling vehicle. First, the vehicle *drives* along its planned route, picking up or dropping off customers on the way [Eq. (2)]. Second, a new customer (red) is assigned to the vehicle, *modifying* the planned route by adding two stops [Eq. (3)]. New stops may be inserted into the planned route or appended at the end, causing detours or extending the planned route further into the future, respectively. (b) Typical ridepooling trajectories driven by a single vehicle for different fleet sizes B and normalized demand (load) q [Eq. (4)]. For larger fleets, trajectories expand. Requests are likely assigned to vehicles with a more similar route, extending routes in the same direction with fewer detours. Conversely, with higher demand q, trajectories contract as more detours are required to pick up and deliver all assigned customers.

processes, we simulate the ridepooling system in a simplified setting. B vehicles with unlimited passenger capacity drive with constant velocity $v = 1$ on the unit square with periodic boundaries. We then unfold their trajectories onto the Euclidean plane [compare Fig. 1(b)]. Requests follow a Poisson process with rate λ in time, with origins distributed uniformly in the unit square and destinations chosen uniformly and isotropically from a disk with radius $1/2$ around the origin of the request, resulting in an average request distance $\langle \ell \rangle = 1/3$. We assign each new request r to a vehicle j^* following a greedy heuristic for the solution of the many-vehicle-routing problem [21]: For each vehicle j and its respective planned route R_j, we identify those positions to insert the pickup and dropoff stops that minimize the vehicle's planned route completion time. The request r is then assigned to that vehicle j^* with the shortest route completion time.

Generalized settings, such as ridepooling on real street topologies [22], yield qualitatively the same results as those presented here for this simplified model.

Two parameters characterize the macroscopic mean-field dynamics of ridepooling [4]. The *load*

$$q = \frac{\lambda \langle \ell \rangle}{vB} \tag{4}$$

is an intensive parameter capturing the relative balance of supply and demand. The load compares the total requested distance per unit time $\lambda \langle \ell \rangle$ to the total distance Bv all ridepooling vehicles drive per unit time. It thus represents a lower bound on the average occupancy of vehicles necessary to serve all requests [4,10]. If $q \leqslant 1$, all requests could, in principle, be served individually. If $q > 1$, pooling rides becomes necessary.

The *fleet size* B describes the extensive size of the ridepooling system, necessary to capture the intrinsic nonlinearity of ridepooling dynamics. For instance, in a system with twice as many vehicles and twice as many requests per time (i.e., at the same load q), a request is more likely to be aligned with the current route of a vehicle. Requests thus are typically assigned with smaller detours, meaning that larger ridepooling systems operate more efficiently [2,5,23].

This effect is also visible in the microscopic vehicle trajectories [Fig. 1(b)]. The larger the load q, the more requests per time are assigned to each vehicle and the more stops are inserted into the planned routes. Individual segments between two stops become shorter and routes become less straight (more random), covering less ground over time. In contrast, the larger the fleet size B (at fixed q), the more vehicles are available to assign requests to, reducing the detours required to insert them into existing routes. The routes deviate less from the directions of the requested trips and therefore remain straighter, covering more ground over time.

How can we link such microscopic routing dynamics to macroscopic properties of a ridepooling system? In the following, we report three core findings that jointly enable such a connection: (1) Ridepooling vehicle trajectories constitute persistent random walks with directional autocorrelation that exhibits three distinct timescales characteristic for the microscopic dynamics of the individual vehicles; (2) the diffusion constant links the microscopic routing dynamics to macroscopic parameters of the ridepooling system; and (3) this connection yields scaling relations for macroscopic observables of service quality that inherently depend on the routing dynamics.

(1) *Persistent random walks.* The autocorrelation

$$\begin{aligned} \rho(\tau) &= \langle \widehat{\partial x}(t+\tau) \cdot \widehat{\partial x}(t) \rangle \\ &= \lim_{T \to \infty} \frac{1}{T} \int_0^T \widehat{\partial x}(t+\tau) \cdot \widehat{\partial x}(t)\, \mathrm{d}t \end{aligned} \tag{5}$$

of the direction $\widehat{\partial x}(t)$ (i.e., the normalized tangent vector) of the driven trajectories quantifies their qualitative differences. The correlation function is approximately

$$\rho(\tau) = w_1\, e^{-\tau/\tau_1} + w_2\, e^{-\tau/\tau_2} + w_3\, e^{-\tau/\tau_3}, \tag{6}$$

with $\tau > 0$ and weights w_n such that $w_1 + w_2 + w_3 = 1$, exhibiting three distinct timescales $\tau_1 \leqslant \tau_2 \leqslant \tau_3$ (Fig. 2).

Initially, the directional correlation decays quickly on a timescale $\tau_{\text{short}} = (\frac{w_1}{\tau_1} + \frac{w_2}{\tau_2} + \frac{w_3}{\tau_3})^{-1}$. This shortest timescale reflects the time a vehicle spends on individual straight route

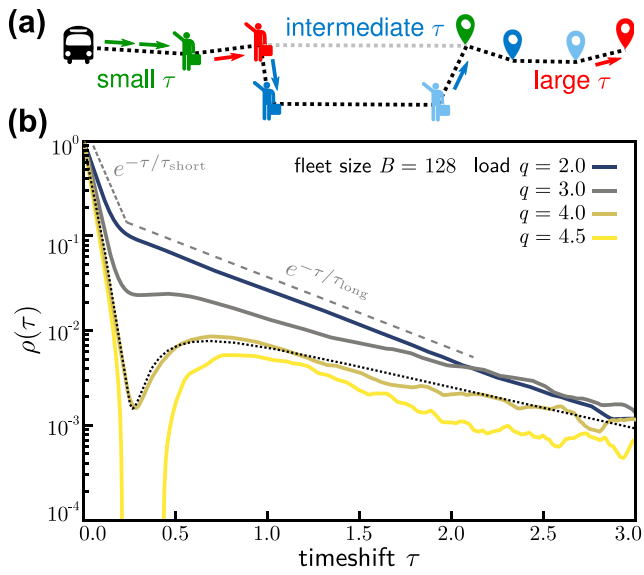

FIG. 2. Correlation functions reveal three timescales in microscopic ridepooling routes. (a) Schematic illustration of the mechanisms underlying the three timescales emerging in the directional correlations of ridepooling trajectories. On short timescales τ, vehicles travel in a straight line between two consecutive stops (green). On intermediate timescales, insertions of new stops induce detours (zigzag patterns) from the original route (blue). On long timescales, new requests preferentially extend the planned route in a direction similar to the overall route (red). (b) Directional correlations of the trajectories of ridepooling vehicles for $B = 128$ vehicles and variable load q reveal three timescales [compare panel (a)]. On short timescales, the correlation decays quickly with a correlation time τ_{short} (gray dotted line). On long timescales, the correlation decays slowly with a correlation time τ_{long} (gray dashed line). As the load q increases (yellow lines compared to blue lines), a third, intermediate timescale emerges where the correlation becomes small or negative. The correlation functions are well described by a sum of three exponentials [Eq. (6)], illustrated by the black dotted line for $q = 4.0$.

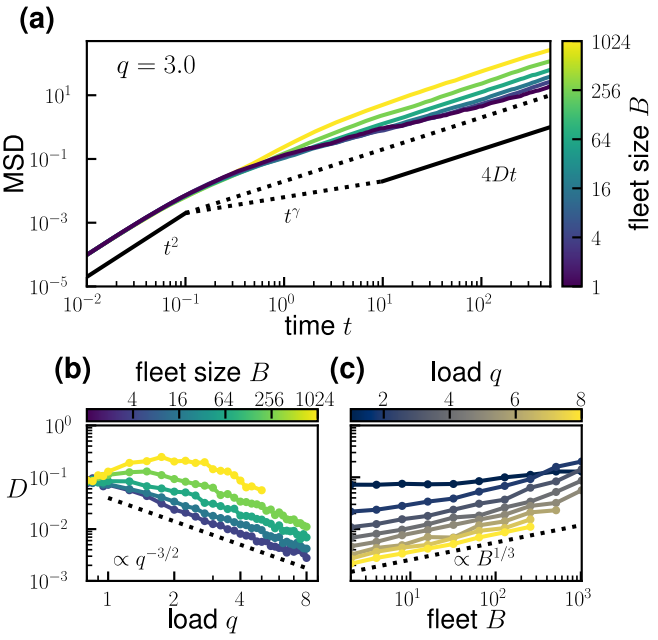

FIG. 3. Diffusion constant connects microscopic dynamics and macroscopic system parameters. (a) The mean squared displacement of ridepooling vehicles (at $q = 3$) is ballistic on short timescales on individual segments of the trajectory, subdiffusive on intermediate timescales due to negative directional correlations (compare Fig. 2), and diffusive with diffusion constant D for long times. The diffusion constant follows power law scaling (b) with the load q and (c) with the fleet size B for sufficiently large load q.

segments between two consecutive stops, analogous to standard random walks with discrete segments [19,20], and is modified by small directional correlations between consecutive segments (see the Supplemental Material [22] for details).

For large delays τ, the correlation decays on a much slower timescale $\tau_{\text{long}} = \tau_3$. New requests are preferentially assigned to vehicles with planned routes that already align with the requested trip direction to avoid detours. Planned routes thus often extend into the same overall direction [compare Fig. 2(a)]. Consequently, the routes remain directed over a long time, similar to persistent random walks [19,20], despite the small directional correlation of consecutive segments captured by τ_{short} (see also the Supplemental Material [22]).

At low loads q, the two timescales τ_{short} and τ_{long} dominate the correlation function. Intriguingly, at higher loads q, a third, intermediate timescale τ_{mid} creates a local minimum in the correlation function [Fig. 2(b)]. With increasing load, more stops are inserted, repeatedly dividing previously existing segments of the route. As the route segments become shorter, the directions of the route to and from the inserted stops tend to become more antiparallel (i.e., the routes exhibit a stronger zigzag pattern), resulting in small or even negative correlations [see Fig. 2(a) and the Supplemental Material [22] for more details]. The same qualitative mechanisms of stop insertion and vehicle routing apply to ridepooling independent of the topology and request distribution, illustrated also for real street networks in the Supplemental Material [22].

(2) *Diffusion constant connects micro- and macroscales.* These directional correlations essentially capture the influence of the microscopic routing dynamics on the average movement of the vehicles [Fig. 3(a)]. On short timescales, along individual segments, the motion of the vehicles is *ballistic*. On intermediate timescales, the motion may be *subdiffusive* for high loads q due to the negative correlations [Fig. 2; see the Supplemental Material [22] for details]. For large times, when directional correlations decay, the trajectory becomes *diffusive*. Notably, with $\vec{x}(t) \in \mathbb{R}^2$, the diffusion constant

$$\begin{aligned} D &= \lim_{t\to\infty} \frac{1}{4t} \langle (\vec{x}(t) - \vec{x}(0))^2 \rangle \\ &= \lim_{t\to\infty} \frac{1}{4t} \int_0^t \int_0^t v^2 \rho(|s - s'|)\, \mathrm{d}s\, \mathrm{d}s' \\ &= \frac{v^2}{2} (\omega_1 \tau_1 + \omega_2 \tau_2 + \omega_3 \tau_3) \end{aligned} \tag{7}$$

does not only depend on the longest timescale of the correlation function but includes information on all timescales underlying the microscopic dynamics [22].

The diffusion constant D simultaneously directly relates to macroscopic system parameters. From extensive direct simulations, we find that for constant fleet size B, the diffusion constant scales as a power law $D \propto q^{-\alpha}$, with $\alpha \approx 3/2$ [Fig. 3(b)]. Similarly, for constant load q, we find that $D \propto B^{\beta}$, with $\beta \approx 1/3$ [Fig. 3(c)]. We thus obtain the combined scaling relation

$$D \propto q^{-\alpha} B^{\beta}, \tag{8}$$

which holds asymptotically for high loads, resulting in relatively small diffusion constants [Figs. 3(b) and 3(c)]. At low loads, $q < 1$, vehicles become idle intermittently and may not have a planned route, qualitatively changing their dynamics (see the Supplemental Material [22]). The scaling relation in Eq. (8) explicitly connects the macroscopic description of the ridepooling dynamics in terms of the load q and the fleet size B with the microscopic routing dynamics captured by the diffusion constant D.

(3) *Scaling laws of macroscopic observables.* In some form, any observable of a ridepooling system inherently depends on the underlying microscopic routing dynamics, characterized by the diffusion constant D on sufficiently long timescales. We find that several key observables quantifying system operations vary with q and B, yet only depend on their combination through the diffusion constant D and thus the combination $q^{-\alpha} B^{\beta}$. For instance, the average velocity

$$v_{\text{eff}} = \langle l_r / \Delta t_r \rangle_r \tag{9}$$

quantifies how efficiently customers are moving, given by the quotient of the direct distance l_r and the service time Δt_r of a trip, averaged over all requests r. Although the effective velocity v_{eff} varies with the load q and the fleet size B (Fig. 4, inset), it collapses to a single scaling function

$$v_{\text{eff}} = f\left(q^{3/2} B^{-1/3}\right) = g(D) \tag{10}$$

of the diffusion constant (Fig. 4, main panel). This scaling relation links the microscopic routing dynamics to macroscopic properties of the ridepooling system via the diffusion constant. We find similar scaling functions for other observables characterizing the long-time dynamics of the ridepooling system, such as the average occupancy or the average number of assigned requests per vehicle (see the Supplemental Material [22]).

Various random walk and diffusion processes have helped to understand a broad range of physical, biological, and technical systems by linking microscopic dynamics and macroscopic observations [20,24,25]. Examples range from the basic theory of Brownian motion [19,26,27] over the structure and dynamics of biological systems and self-propelled particles [20,28–32] to stochastic fluctuations in energy and financial markets [33,34] and models of human mobility [25,35,36].

Our results provide first key insights on the explicit connection between the microscopic vehicle trajectories and macroscopic observables in ridepooling systems and enable us to understand their features beyond existing mean-field approaches or case-by-case simulations [2,4,9,15,17]. The insights, thus, not only open up novel perspectives for the theory of random walks but may equally help improve our understanding of ridepooling, for instance, by identifying the

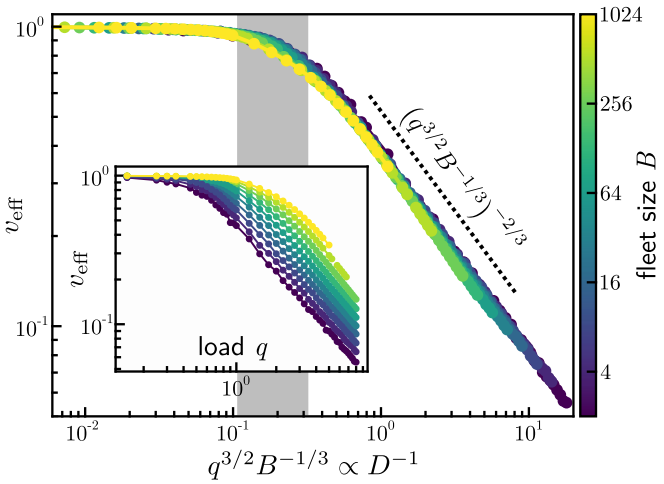

FIG. 4. Scaling law of ridepooling observables characterizes system efficiency. (Inset) Macroscopic observables, like the average effective velocity of customers [Eq. (9)], depend on both the number of vehicles B and the load q of the system. A transition from fast, direct trips in a taxilike regime, $v_{\text{eff}} \approx 1$, to shared trips with larger detours, $v_{\text{eff}} \ll 1$, occurs at different loads for different fleet sizes. (Main panel) Plotting the same observable v_{eff} as a function of q and B according to the scaling of the diffusion constant [Eq. (8)] collapses all observations to a single curve, illustrating the connection of the microscopic routing dynamics to macroscopic observables (see the Supplemental Material [22] for additional examples). The results indicate that the transition (gray area) between taxilike services (left) and true ridepooling (right) is determined by the combination $q^{-\alpha} B^{\beta}$.

fleet size required (Fig. 4) for a given load (4) that follows from the demand patterns and characteristic vehicle velocities.

We note that, commonly, subdiffusion is due to waiting events, crowding, or other local physical constraints, such as system boundaries. Our results indicate that subdiffusion may also emerge without such physical constraints: Inserting many new stops into a preplanned route deteriorates its overall directional alignment, such that sequences of route segments become increasingly zigzag-shaped. These mechanisms generalize beyond the basic setting we have focused on above. In particular, short- and long-term alignment and intermediate-time detours underlying the three timescales analogously emerge in systems operating on street networks, systems with limited passenger capacity, or inhomogeneous demand patterns and vehicle properties, as, for instance, illustrated in the Supplemental Material [22] for ridepooling simulations on the street network of Manhattan with empirical demand data (compare also Refs. [4,22,37,38]).

The rise of digitization and on-demand services may make random walks with preplanned future trajectories increasingly relevant for various human-designed sociotechnical systems, for example, mobility and logistics services with planned and dynamic deliveries [13,14,39,40] or electricity markets with scheduled and irregular transactions [41–43]. Further understanding the impact of partially predetermined dynamics may thus not only widen our theoretical concepts about such processes but also support a range of novel applications beyond ridepooling.

We thank Benjamin Köhler and Benjamin Friedrich for helpful comments and discussions. This research was partially supported by the German Federal Ministry for Education and Research (BMBF) under Grant No. 16ICR01 and by the German Federal Ministry for Digital and Transport (BMDV) as part of the innovation initiative mFund under Grant No. 19F1155A. This research was supported through the Center for Advancing Electronics Dresden (CFAED). The authors are grateful to the Center for Information Services and High Performance Computing (ZIH) TU Dresden for providing facilities for high-throughput calculations.

Data sets generated during the current study are available from the corresponding author on reasonable request.

[1] P. Santi, G. Resta, M. Szell, S. Sobolevsky, S. H. Strogatz, and C. Ratti, Quantifying the benefits of vehicle pooling with shareability networks, Proc. Natl. Acad. Sci. USA **111**, 13290 (2014).

[2] R. Tachet, O. Sagarra, P. Santi, G. Resta, M. Szell, S. H. Strogatz, and C. Ratti, Scaling law of urban ride sharing, Sci. Rep. **7**, 42868 (2017).

[3] M. M. Vazifeh, P. Santi, G. Resta, S. H. Strogatz, and C. Ratti, Addressing the minimum fleet problem in on-demand urban mobility, Nature **557**, 534 (2018).

[4] N. Molkenthin, M. Schröder, and M. Timme, Scaling laws of collective ride-sharing dynamics, Phys. Rev. Lett. **125**, 248302 (2020).

[5] D.-M. Storch, M. Timme, and M. Schröder, Incentive-driven discontinuous transition to high ride-sharing adoption, Nat. Commun. **12**, 3003 (2021).

[6] H. Wolf, D.-M. Storch, M. Timme, and M. Schröder, Spontaneous symmetry breaking in ride-sharing adoption dynamics, Phys. Rev. E **105**, 044309 (2022).

[7] C. Lotze, P. Marszal, M. Schröder, and M. Timme, Dynamic stop pooling for flexible and sustainable ride sharing, New J. Phys. **24**, 023034 (2022).

[8] W. Li, Z. Pu, Y. Li, and M. Tu, How does ridesplitting reduce emissions from ridesourcing? A spatiotemporal analysis in Chengdu, China, Transp. Res. D **95**, 102885 (2021).

[9] J. Alonso-Mora, S. Samaranayake, A. Wallar, E. Frazzoli, and D. Rus, On-demand high-capacity ride-sharing via dynamic trip-vehicle assignment, Proc. Natl. Acad. Sci. USA **114**, 462 (2017).

[10] C. Lotze, P. Marszal, F. Jung, D. Manik, M. Timme, and M. Schröder, Identifying the threshold to sustainable ridepooling, arXiv:2306.05851.

[11] D. Manik and N. Molkenthin, Topology dependence of on-demand ride-sharing, Appl. Netw. Sci. **5**, 49 (2020).

[12] A. Fielbaum, M. Kronmueller, and J. Alonso-Mora, Anticipatory routing methods for an on-demand ridepooling mobility system, Transportation **49**, 1921 (2022).

[13] A. Fielbaum and J. Alonso-Mora, Design of mixed fixed-flexible bus public transport networks by tracking the paths of on-demand vehicles, Transp. Res. C **168**, 104580 (2024).

[14] K. M. Mittal, M. Timme, and M. Schröder, Efficient self-organization of informal public transport networks, Nat. Commun. **15**, 4910 (2024).

[15] F. Zwick, N. Kuehnel, R. Moeckel, and K. W. Axhausen, Agent-based simulation of city-wide autonomous ride-pooling and the impact on traffic noise, Transp. Res. D **90**, 102673 (2021).

[16] R. Engelhardt, F. Dandl, A. Bilali, and K. Bogenberger, Quantifying the benefits of autonomous on-demand ride-pooling: A simulation study for Munich, Germany, in *Proceedings of the 2019 IEEE Intelligent Transportation Systems Conference (ITSC)* (IEEE, Auckland, New Zealand, 2019), p. 2992.

[17] S. Herminghaus, Mean field theory of demand responsive ride pooling systems, Transp. Res. A **119**, 15 (2019).

[18] P. Sharma, K. M. Heidemann, H. Heuer, S. Mühle, and S. Herminghaus, Sustainable and convenient: Bi-modal public transit systems outperforming the private car, Multimodal Transp. **2**, 100083 (2023).

[19] J. Rudnick and G. Gaspari, *Elements of the Random Walk: An Introduction for Advanced Sudents and Researchers* (Cambridge University Press, Cambridge, UK, 2004).

[20] H. C. Berg, *Random Walks in Biology* (Princeton University Press, Princeton, 2018).

[21] Google OR-Tools, Integer programming and routing solver, https://developers.google.com/optimization.

[22] See Supplemental Material at http://link.aps.org/supplemental/10.1103/bjqt-5vkq for additional details on the routing dynamics on short and medium timescales, scaling laws with the diffusion constant, and robustness of the results for dynamics on real street networks.

[23] A. Fielbaum, A. Tirachini, and J. Alonso-Mora, Economies and diseconomies of scale in on-demand ridepooling systems, Econ. Transp. **34**, 100313 (2023).

[24] V. Zaburdaev, S. Denisov, and J. Klafter, Lévy walks, Rev. Mod. Phys. **87**, 483 (2015).

[25] H. Barbosa, M. Barthelemy, G. Ghoshal, C. R. James, M. Lenormand, T. Louail, R. Menezes, J. J. Ramasco, F. Simini, and M. Tomasini, Human mobility: Models and applications, Phys. Rep. **734**, 1 (2018).

[26] A. Einstein, Über die von der molekularkinetischen Theorie der Wärme geforderte Bewegung von in ruhenden Flüssigkeiten suspendierten Teilchen, Ann. Phys. **322**, 549 (1905).

[27] M. von Smoluchowski, Zur kinetischen theorie der Brownschen molekularbewegung und der suspensionen, Ann. Phys. **326**, 756 (1906).

[28] P. J. Flory, *Principles of Polymer Chemistry* (Cornell University Press, Ithaca, 1953).

[29] R. A. L. Jones, *Soft Condensed Matter* (Oxford University Press, Oxford, 2002).

[30] J. R. Howse, R. A. L. Jones, A. J. Ryan, T. Gough, R. Vafabakhsh, and R. Golestanian, Self-motile colloidal particles: From directed propulsion to random walk, Phys. Rev. Lett. **99**, 048102 (2007).

[31] C. Kurzthaler, Y. Zhao, N. Zhou, J. Schwarz-Linek, C. Devailly, J. Arlt, J.-D. Huang, W. C. K. Poon, T. Franosch, J. Tailleur, and V. A. Martinez, Characterization and control of the run-and-tumble dynamics of *Escherichia coli*, Phys. Rev. Lett. **132**, 038302 (2024).

[32] G. Passucci, M. E. Brasch, J. H. Henderson, V. Zaburdaev, and M. L. Manning, Identifying the mechanism for superdiffusivity

in mouse fibroblast motility, PLoS Comput. Biol. **15**, e1006732 (2019).

[33] O. Peters, The ergodicity problem in economics, Nat. Phys. **15**, 1216 (2019).

[34] E. F. Fama, Random walks in stock market prices, Financ. Anal. J. **51**, 75 (1995).

[35] D. Brockmann, L. Hufnagel, and T. Geisel, The scaling laws of human travel, Nature (London) **439**, 462 (2006).

[36] C. Song, T. Koren, P. Wang, and A.-L. Barabási, Modelling the scaling properties of human mobility, Nat. Phys. **6**, 818 (2010).

[37] R. M. Zech, N. Molkenthin, M. Timme, and M. Schröder, Collective dynamics of capacity-constrained ride-pooling fleets, Sci. Rep. **12**, 10880 (2022).

[38] D. Kondor, I. Bojic, G. Resta, F. Duarte, P. Santi, and C. Ratti, The cost of non-coordination in urban on-demand mobility, Sci. Rep. **12**, 4669 (2022).

[39] *The Vehicle Routing Problem: Latest Advances and New Challenges*, edited by B. L. Golden, S. Raghavan, and E. A. Wasil (Springer, New York City, 2008).

[40] Y. Huang, L. Zhao, T. Van Woensel, and J.-P. Gross, Time-dependent vehicle routing problem with path flexibility, Transp. Res. B **95**, 169 (2017).

[41] M. Mureddu and H. Meyer-Ortmanns, Extreme prices in electricity balancing markets from an approach of statistical physics, Physica A **490**, 1324 (2018).

[42] B. Schäfer, C. Beck, K. Aihara, D. Witthaut, and M. Timme, Non-Gaussian power grid frequency fluctuations characterized by Lévy-stable laws and superstatistics, Nat. Energy **3**, 119 (2018).

[43] C. Han, H. Hilger, E. Mix, P. C. Böttcher, M. Reyers, C. Beck, D. Witthaut, and L. R. Gorjão, Complexity and persistence of price time series of the European electricity spot market, PRX Energy **1**, 013002 (2022).